D.A. Dei Tos, F. Topputo
On the Advantages of Exploiting the Hierarchical Structure of Astrodynamical Models
Acta Astronautica, Vol. 136, 2017, p. 236-247
doi:10.1016/j.actaastro.2017.02.025

On the advantages of exploiting the hierarchical structure of astrodynamical models

Diogene Alessandro Dei Tos[a,*], Francesco Topputo[b]

[a]*Ph.D. candidate, Department of Aerospace Science and Technology, Politecnico di Milano, via la Masa 34, 20156, Milan, Italy.*
[b]*Assistant Professor, Department of Aerospace Science and Technology, Politecnico di Milano, via la Masa 34, 20156, Milan, Italy.*

Abstract

In this paper an algorithm is developed that combines the capabilities and advantages of several different astrodynamical models of increasing complexity. Splitting these models in a strict hierarchical order yields a clearer grasp on what is available. With the effort of developing a comprehensive model overhead, the equations for the spacecraft motion in simpler models can be readily obtained as particular cases. The proposed algorithm embeds the circular and elliptic restricted three-body problems, the four-body bicircular and concentric models, an averaged n-body model, and, at the top hierarchic ladder, the full ephemeris SPICE-based restricted n-body problem. The equations of motion are reduced to the assignment of 13 time-varying coefficients, which multiply the states and the gravitational potential to reproduce the proper vector field. This approach yields an efficient and quick way to check solutions for different dynamics and parameters. We show that in bottom-up applications, a gradual increase of model complexity benefits accuracy, the chances of success and the convergence rate of a continuation algorithm. Case studies are simple periodic orbits and low-energy transfers.

Keywords: n-body dynamics, four-body problem, three-body problem

1. INTRODUCTION

The circular restricted three-body problem, addressed CRTBP later in this work, is the ideal model to design unique solutions, ranging from Lagrange point orbits to low energy transfers [5, 12, 25]. These trajectories embed the effect of two gravitational attractions in a natural way, and therefore they are more accurate than the conics, solutions of the classic two-body problem. The phase space portrait of the CRTBP has been thoroughly studied in the past, with special attention to the dynamics in the neighbourhood of the collinear libration points [21, 15, 12]. This is because most of the dynamics of the restricted problem can be related to the equilibrium points and their invariant stable and unstable manifolds. From a practical perspective, these points possess properties that make them valuable candidates for space missions. Herschel, Planck and Gaia about the Sun–Earth L_2, and SOHO and Genesis about Sun–Earth L_1, are just few examples of typical libration points missions. Several other missions are planned that make explicit use of three-body dynamics, such as Plato and Euclid. Finally, the concepts of weak stability boundaries and ballistic capture [11, 19, 26], proved reliable from the rescue of the Japanese spacecraft Hiten [2], and will be applied to the ESA's cornerstone mission BepiColombo [20].

However, when the three-body orbits are reproduced in more comprehensive gravitational models, large errors are found. That is, as the three-body orbits are defined in the regions of phase space where two main gravitational accelerations balance, the sensitivity is high and any additional perturbation produces large effects. An automatic algorithm able to correct orbits in the real solar system model is in these circumstances of great aid to space mission design [9].

Several works exist in literature that present a way to account for the full gravitational dynamics of the solar system. Dynamical substitutes are found by continuation in [14] and [15]; through a reduction to the centre manifold and by numerically imposing the solution to be quasi-periodic in [12]; or selecting a finite number of frequencies that reasonably represents the major contribution of the celestial bodies [13]. Corrections have also been obtained retaining a very large number of frequencies in an analytical power series expansion of the gravitational potential [17].

The purpose of this paper is to establish a clear hierarchy in the gravitational models available to the designer, and to explicitly exploit it for the continuation of typical three-body orbits in the n-body problem, modelled through precise ephemeris data. To achieve the objective, an automatic algorithm has been implemented. This combines the capabilities and advantages of several different astrodynamical models of increasing complexity. Splitting these models in a strict hierarchical order allows a clearer grasp on what is available. The differential equations governing the dynamics of a massless particle within the vector field generated by the n celestial bodies in the solar system are written as perturbation of the CRTBP in a non-uniformly rotating and pulsating frame. In this way, the equations for the spacecraft motion in simpler models can be readily obtained as particular cases of those in the general model. The equations of motion are reduced to the assignment of 13 time-varying coeffi-

*Corresponding author
Email address: diogenealessandro.deitos@polimi.it (Diogene Alessandro Dei Tos)

cients, which multiply the states and the gravitational potential to reproduce the proper vector field.

The refinement is carried out by means of a modified multiple shooting technique, and the problem is solved for a finite set of variables. The proposed approach allows checking solutions for different dynamics and parameters in an efficient and quick way. It is shown how a gradual increase of the dynamics complexity benefits accuracy, the chances of success and the convergence rate of a continuation algorithm, applied to simple periodic orbits and low-energy transfers.

The approach used in this work possesses similar traits compared to the one developed in [22] and [28]. Nonetheless, the explicit exploitation of a gravitational hierarchy in the models represents a new approach. The results of the Earth–Moon system serve as solid benchmark to validate this procedure compared to others and prove this method correct and reliable. The results obtained in this work further improve the algorithm developed in [8] and [15].

This paper is organised as follows. In Section 2 the dynamical models that are used for the numerical computations are described, paying careful attention to their hierarchical order. Section 3 is the core of this work and details the algorithm that refines trajectories in the real solar system model. The methodology and numerical procedure are explained. The results are illustrated and discussed in Section 4, where families of halo orbits and one example of low-energy transfer are corrected with the proposed algorithm. Conclusions are drawn in Section 5.

2. DYNAMICAL MODELS

A great variety of astrodynamical models are available to the designer. As the complexity of such models increases, new solutions appear due to the richer content of the vector field. The drawback is that no analytical solution is available, and consequently it's very difficult to have a general insight on the dynamics. Extensive computational searches are usually required in order to hit the desired optimal trajectory.

In this section the main astrodynamical models are shown to be a particular case of the roto-puslating n-body problem. With this approach, a single set of equations can be used to represent the whole domain of possible gravitational models, simply varying the coefficients and the potential function of the model on the top of the hierarchic ladder.

2.1. The problem of n bodies

The most general model for the description of the motion of a massless particle subjected to the gravitational field of other $n-1$ celestial bodies is the n-body problem, whose geometry is shown in Figure 1. The dynamics of the particle P_k of mass $m_k, k = 1,\ldots,n$, whose Cartesian coordinates are $\mathbf{R}_k = (X_k, Y_k, Z_k)^T$ is governed by Newton's universal law of gravitation:

$$m_k\ddot{\mathbf{R}}_k = \sum_{\substack{j=1\\ j\neq k}}^{j=n} \frac{Gm_jm_k}{R_{jk}^3}(\mathbf{R}_j - \mathbf{R}_k) \qquad k = 1,\ldots,n \qquad (1)$$

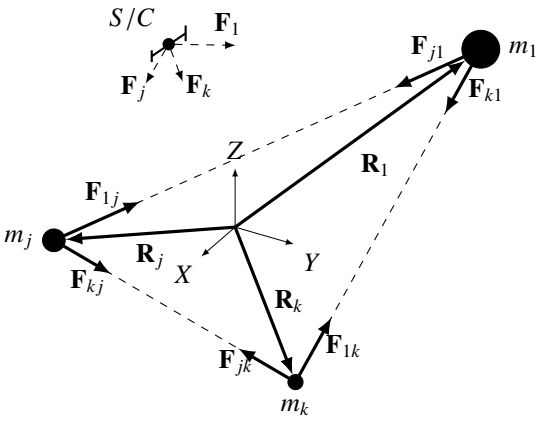

Figure 1: Geometry of the n-body problem in an inertial reference frame.

Eq. (1) is written in an inertial reference frame and represents a set of $6n$ first order ordinary differential equations.

However, astrodynamics is mainly concerned with the study of artificial objects. In this context, the hypothesis of restricted dynamics is applied with accurate results. The artificial object moves in the vector field created by the $n-1$ celestial bodies, without affecting their motion. Another significant simplification can be obtained if the trajectories of the primaries are not integrated, rather they are specified by proper time-dependent functions. Let $\mathcal{S}$ be the set of celestial bodies, the motion of an artificial satellite is represented by

$$\ddot{\mathbf{R}} = \sum_{j\in\mathcal{S}} \mu_j \frac{\mathbf{R}_j - \mathbf{R}}{\|\mathbf{R}_j - \mathbf{R}\|^3}, \qquad (2)$$

where $\mu_j = Gm_j$ is the j-th body mass parameter, G is the universal constant of gravitation, and $\mathbf{R} = (X, Y, Z)^T$ is the position of the probe.

We avail ourselves of the JPL ephemeris data DE430 [10] to determine in a precise way the states of the Sun, the planets and the Moon at given epochs with respect to an inertial reference frame whose origin is located at the solar system barycentre. More precisely, the SPICE toolkit[1] has been use to determine the states of the celestial bodies.

The equations of the solar system restricted n-body problem, or simply SSRnBP, are written as perturbation of the CRTBP, by means of a time-dependent coordinates transformation [13]; in this way a better insight of each term can be attained. Moreover, this model fits well in the hierarchic approach followed in this paper. Let $\boldsymbol{R}$ and $\boldsymbol{V}$ be the dimensional position and velocity, respectively, of a massless body P in the inertial solar system barycentric frame, and let $\boldsymbol{\rho}$ be its nondimensional position in the new rotating and pulsating reference frame, defined by a pair of primaries P_1 and P_2 (see Fig. 2). The transformation between the solar system barycentric reference frame, and the new non-inertial reference is then

$$\mathbf{R} = \mathbf{b} + kC\boldsymbol{\rho}, \qquad (3)$$

[1] The toolkit is freely available through the NASA NAIF website. Please refer to `http://naif.jpl.nasa.gov/naif/`. Downloaded on Dec 22 2016.

where

$$\begin{aligned} \mathbf{b}(t) &= \frac{m_1\mathbf{R}_1 + m_2\mathbf{R}_2}{m_1 + m_2}, \\ k(t) &= \|\boldsymbol{R}_2 - \boldsymbol{R}_1\|, \\ C(t) &= [\mathbf{e}_1, \mathbf{e}_2, \mathbf{e}_3], \end{aligned} \tag{4}$$

and

$$\begin{cases} \mathbf{e}_1 = \dfrac{\boldsymbol{R}_2 - \boldsymbol{R}_1}{k}, \\ \mathbf{e}_2 = \mathbf{e}_3 \times \mathbf{e}_1, \\ \mathbf{e}_3 = \dfrac{(\boldsymbol{V}_2 - \boldsymbol{V}_1) \times (\boldsymbol{R}_2 - \boldsymbol{R}_1)}{\|(\boldsymbol{V}_2 - \boldsymbol{V}_1) \times (\boldsymbol{R}_2 - \boldsymbol{R}_1)\|}. \end{cases} \tag{5}$$

In Eq. (4) and Eq. (5), m_i, $\boldsymbol{R}_i$, and $\boldsymbol{V}_i$ are the mass, position, and velocity of P_i, respectively, $i = 1, 2$. The transformation is hence composed by two parts. The first is a translation of the origin from the solar system barycentre to the primaries centre of mass, $\mathbf{b}$. The second is a rotation by means of the orthogonal cosine angle matrix C, and a scaling by means of the time-dependent factor k. The rotation is such that the primaries are always aligned with the x-axis of the new frame. The scaling factor k, which is the actual distance between the primaries, adjusts their positions so as to be fixed in time with respect to the new frame of reference. As a result, the new frame rotates and pulsates in a non-uniform fashion. This guarantees some convenient features, primarily suggested by the CRTBP. In this paper the new gravitational model will be addressed as *roto-pulsating n-body problem*, or simply RPnBP.

The Lagrangian of the complete gravitational model is:

$$\mathscr{L}(\mathbf{R}, \dot{\mathbf{R}}, t) = T - V = \frac{1}{2}\dot{\mathbf{R}} \cdot \dot{\mathbf{R}} + \sum_{j \in \mathcal{S}} \frac{Gm_j}{\|\mathbf{R} - \mathbf{R}_j\|}, \tag{6}$$

where $\mathcal{S}$ is the set of all celestial bodies included in the solar system model, except for P. The dots indicate derivation with respect to dimensional time, t.

Without loss of generality, a constant time reference is chosen for the nondimensionalisation, equal to the mean motion of the primaries, n. With this choice the average primaries revolution period is 2π, that is

$$\tau = n(t - t_0), \qquad n = \frac{2\pi}{T} = \sqrt{\frac{G(m_1 + m_2)}{\bar{a}^3}}, \tag{7}$$

where $\bar{a}$ is the mean distance between the primaries taken over a long time interval (e. g., 400 years). Note that the mean distance between primaries is not the semi-major axis of the ellipse described by their orbits, the eccentricity modifies it by a factor $\sqrt{1 - e^2}$. The initial epoch t_0 is used to shift the non autonomous problem to have null initial nondimensional time.

Applying the transformation of Eq. (3) to the Lagrangian (Eq. (6)), and then carrying out the Lagrangian mechanics operations, we obtain the equations of motion in the roto-pulsating frame. After some manipulation [7]:

$$\begin{aligned} \boldsymbol{\rho}'' = &-\frac{2}{n}\left(\frac{\dot{k}}{k}\mathcal{I} + C^T\dot{C}\right)\boldsymbol{\rho}' - \frac{1}{n^2}\left[\left(\frac{\ddot{k}}{k}\mathcal{I} + 2\frac{\dot{k}}{k}C^T\dot{C}\right.\right. \\ &\left.\left. + C^T\ddot{C}\right)\boldsymbol{\rho} + \frac{1}{k}C^T\ddot{\mathbf{b}}\right] + \frac{\mu_1 + \mu_2}{n^2k^3}\nabla\Omega, \end{aligned} \tag{8}$$

in which primes indicate derivatives with respect to the nondimensional time, τ, and $\nabla\Omega$ is the gradient of the potential function of the RPnBP

$$\Omega = (1 - \mu)\frac{\boldsymbol{\rho} - \boldsymbol{\rho}_1}{\|\boldsymbol{\rho} - \boldsymbol{\rho}_1\|^3} + \mu\frac{\boldsymbol{\rho} - \boldsymbol{\rho}_2}{\|\boldsymbol{\rho} - \boldsymbol{\rho}_2\|^3} + \sum_{j \in \mathcal{S}^*} \hat{\mu}_j \frac{\boldsymbol{\rho} - \boldsymbol{\rho}_j}{\|\boldsymbol{\rho} - \boldsymbol{\rho}_j\|^3}, \tag{9}$$

where $\mathcal{S}^*$ is the collection of celestial bodies except for the primaries, and $\hat{\mu}_j = m_j/(m_1 + m_2)$ is a convenient form to express their mass parameters. Mixed derivative notation stems acknowledging that ephemeris data is numeric, discrete, and provided for regular dimensional time. The vector Eq. (8) might be written per components,

$$x'' = b_1 + b_4x' + b_5y' + b_7x + b_9y + b_8z + b_{13}\Omega_{/x}, \tag{10a}$$

$$y'' = b_2 - b_5x' + b_4y' + b_6z' - b_9x + b_{10}y + b_{11}z + b_{13}\Omega_{/y}, \tag{10b}$$

$$z'' = b_3 - b_6y' + b_4z' + b_8x - b_{11}y + b_{12}z + b_{13}\Omega_{/z}, \tag{10c}$$

with coefficients

$$\begin{aligned} b_1 &= -\frac{\ddot{\mathbf{b}} \cdot \mathbf{e}_1}{kn^2}, & b_7 &= -\frac{1}{n^2}\left(\frac{\ddot{k}}{k} - \dot{\mathbf{e}}_1 \cdot \dot{\mathbf{e}}_1\right), \\ b_2 &= -\frac{\ddot{\mathbf{b}} \cdot \mathbf{e}_2}{kn^2}, & b_8 &= \frac{1}{n^2}\dot{\mathbf{e}}_1 \cdot \dot{\mathbf{e}}_3, \\ b_3 &= -\frac{\ddot{\mathbf{b}} \cdot \mathbf{e}_3}{kn^2}, & b_9 &= \frac{1}{n^2}\left(2\frac{\dot{k}}{k}\mathbf{e}_2 \cdot \dot{\mathbf{e}}_1 + \mathbf{e}_2 \cdot \ddot{\mathbf{e}}_1\right), \\ b_4 &= -\frac{2}{n}\frac{\dot{k}}{k}, & b_{10} &= -\frac{1}{n^2}\left(\frac{\ddot{k}}{k} - \dot{\mathbf{e}}_2 \cdot \dot{\mathbf{e}}_2\right), \\ b_5 &= \frac{2}{n}\mathbf{e}_2 \cdot \dot{\mathbf{e}}_1, & b_{11} &= \frac{1}{n^2}\left(2\frac{\dot{k}}{k}\mathbf{e}_3 \cdot \dot{\mathbf{e}}_2 + \mathbf{e}_3 \cdot \ddot{\mathbf{e}}_2\right), \\ b_6 &= \frac{2}{n}\mathbf{e}_3 \cdot \dot{\mathbf{e}}_2, & b_{12} &= -\frac{1}{n^2}\left(\frac{\ddot{k}}{k} - \dot{\mathbf{e}}_3 \cdot \dot{\mathbf{e}}_3\right), \\ b_{13} &= \frac{\mu_S + \mu_P}{k^3n^2}. \end{aligned} \tag{11}$$

These are the equations used throughout this work. Note that a straightforward balance between centrifugal and gravitational

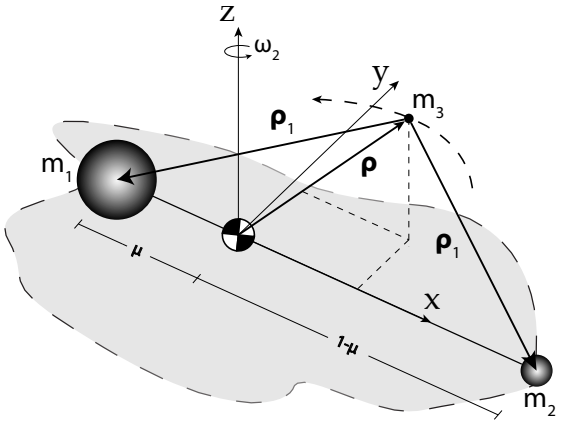

Figure 2: Roto-pulsating reference frame.

forces would require the coefficient b_{13} to be unity when considering just two main bodies (i. e., the CRTBP). In the general case this coefficient will oscillate about this value due to the variability of k.

2.2. Circular restricted three-body problem

The lower level in the hierarchic ladder is represented by the circular restricted three-body problem. Let us consider a body P of mass m in the vector field of two primaries P_1, P_2 of masses m_1 and m_2, respectively, such that the condition $m \ll m_2 < m_1$ is satisfied. In the CRTBP the primaries revolve in planar configuration at constant angular speed. By means of a proper nondimensionalisation [27] the equations of motion depend only on the mass parameter, $\mu = m_2/(m_1 + m_2)$. The nondimensionalisation is such that the distance between the primaries, their angular speed and the sum of their masses are set to a unity value. In this system the positions of P_1 and P_2 are fixed, being P_1 located at $(-\mu, 0, 0)$ and P_2 at $(1-\mu, 0, 0)$. The equations of motion read

$$\ddot{x} - 2\dot{y} = \Omega^{(3)}_{/x}, \qquad \ddot{y} + 2\dot{x} = \Omega^{(3)}_{/y}, \qquad \ddot{z} = \Omega^{(3)}_{/z}, \tag{12}$$

where the three-body potential function can be expressed as

$$\Omega^{(3)} = \frac{1}{2}(x^2 + y^2) + \frac{1-\mu}{r_1} + \frac{\mu}{r_2} + \frac{1}{2}\mu(1-\mu), \tag{13}$$

and terms $r_1 = \sqrt{(x+\mu)^2 + y^2 + z^2}$ and $r_2 = \sqrt{(x-1+\mu)^2 + y^2 + z^2}$ are the scalar distances between the third mass and the primaries.

The dynamic equations describing this model can hence be seen as a particular case of the more general RPnBP, and are indeed obtained by simply assigning proper values to the coefficients, i. e., $b_i = 0$ for $i \neq [5, 7, 10, 13]$, $b_5 = 2$, and $b_7 = b_{10} = b_{13} = 1$.

2.3. Elliptic restricted three-body problem

The next step in the hierarchy is the elliptic restricted three-body problem, or ERTBP. This model studies the motion of a massless particle, P, under the gravitational field generated by the mutual elliptic motion of two primaries, P_1 and P_2, of masses m_1, m_2, respectively. The equations of motion for P are [27]

$$x'' - 2y' = \omega_{/x}, \qquad y'' + 2x' = \omega_{/y}, \qquad z'' = \omega_{/z}. \tag{14}$$

The subscripts in Eq. (14) mean the partial derivative of

$$\omega(x, y, z, f) = \frac{\Omega^{(3)} - \frac{1}{2}z^2 e_p \cos f}{1 + e_p \cos f}, \tag{15}$$

where the potential function is the same defined in the CRTBP, Eq. (13). Primes denote derivatives with respect to the new independent variable: the true anomaly, f.

Eqs. (14) are written in a non uniformly rotating, barycentric, nondimensional coordinate frame where P_1 and P_2 have fixed positions $(-\mu, 0, 0)$ and $(1-\mu, 0, 0)$, respectively, and μ is the mass parameter of the system. This coordinate frame isotropically pulsates as the P_1P_2 distance, assumed to be the unit length. It varies according to the mutual position of the two primaries with respect to f, the true anomaly of the system. This is the independent variable and plays the role of time: f is equal to zero when P_1, P_2 are at their periapsides, as both primaries orbits their barycentre in similarly oriented ellipses having common eccentricity e_p. Normalising the primaries period to 2π, the dependence of true anomaly on time is

$$\frac{df}{dt} = \frac{(1 + e_p \cos f)^2}{(1 - e_p)^{3/2}}. \tag{16}$$

Unlike the CRTBP, the true anomaly in Eq. (15) makes the elliptic problem nonautonomous. Thus, any qualitative feature of this problem strictly depends on the true anomaly, f.

The coefficients of the elliptic restricted three-body problem are not constant, but depend on the true anomaly. Namely,

$$\begin{aligned} b_5 &= 2, \qquad b_{12} = -\frac{e_p \sin f}{1 + e_p \cos f}, \\ b_7 &= b_{10} = b_{13} = \frac{1}{1 + e_p \cos f}. \end{aligned} \tag{17}$$

Note that these coefficients reduce to those of the CRTBP if the eccentricity of the primaries is zero, i. e., $e_p = 0$.

2.4. Restricted four-body problem

Including an additional massive body into the bargain can potentially lead to a different dynamical behaviour and solutions. As the geometry becomes more complex, so does the hierarchical ladder. There is a bifurcation of models at this point: 1) a system of two bodies revolves about a massive celestial body in the bicircular model; or 2) two bodies revolve in similar fashion around a massive primary in the concentric model.

2.4.1. Bicircular four-body model

The bicircular problem, addressed BCP hereafter, is a restricted non-coherent model that considers two primaries and a third gravitational perturbation:

1. two primaries P_1 and P_2 (e. g., the Earth and the Moon) revolve in circular orbits around their barycentre, B;
2. at the same time, B and the third body P_3 (e. g., the Sun) are moving in circular orbits around the centre of masses of the whole system (e. g., Earth–Moon–Sun), B';
3. the primaries and the third body moves in the same plane.

For the sake of clarity the system Earth–Moon–Sun is analysed here. The results can be easily generalised and extended to other selection of primaries with proper adjustments in the model parameters. Fig. 3 shows the geometry of the BCP. Beginning with an inertial frame, we perform a change of variables to write the equations in synodical Earth–Moon coordinates. However, in this case attention must be exerted in the transformation since the Earth–Moon barycentre ceases to be an inertial point, due to the perturbation of the third body. From Newton's

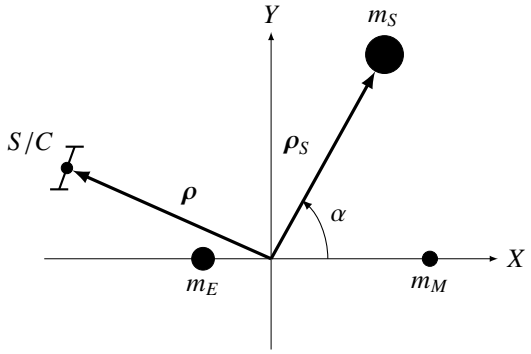

Figure 3: Geometry of the BCP in rotating Earth–Moon coordinates.

law, the derivation of the equations of motion for a massless particle P is straightforward. The nondimensionalistaion paradigm closely follows the one used for the CRTBP: it is such that the distance between the primaries, their angular speed and the sum of their masses are set to a unity value. In this system the positions of P_1 and P_2 are fixed, P_1 being located at $(-\mu, 0, 0)$ and P_2 at $(1-\mu, 0, 0)$. To properly define the dynamics of the fourth body in nondimensional coordinates, new quantities have to be introduced: the Sun mass, m_3, the distance between the Earth–Moon barycentre and the Sun, a_3, and the mean angular velocity of the Sun in inertial and synodic coordinates, n_3 and ω_3. These quantities are not independent. The following equalities hold:

$$\omega_3 = n_3 - 1, \qquad a_3^3 n_3^2 = 1 + m_3, \qquad \alpha = \omega_3 t. \tag{18}$$

The first one is easy to understand since the angular velocity of the synodic frame is 1. The second is a consequence of the third Kepler's law in nondimensional coordinates. In the third equality, α is the phase angle between the Earth–Moon line and the Sun (see Fig. 3). The values used for these quantities are [1]

$$a_3 = 388.81114, \quad \omega_3 = -0.9251959855, \quad m_3 = 328900.54. \tag{19}$$

With these parameters the position of the Sun in the Earth–Moon synodic frame can be written as

$$\boldsymbol{\rho}_S = a_S \begin{bmatrix} \cos(\alpha + \alpha_0) & \sin(\alpha + \alpha_0) & 0 \end{bmatrix}^T, \tag{20}$$

where α_0 is the initial phase angle of the Sun, which depends on the initial epoch and makes the BCP nonautonomous.

The equations of motion read

$$\begin{aligned} \boldsymbol{\rho}'' + C^T(2C'\boldsymbol{\rho}' + C''\boldsymbol{\rho}) = (\mu_2 - 1)\Bigg[& -\frac{\boldsymbol{\rho} - \boldsymbol{\rho}_S}{\|\boldsymbol{\rho} - \boldsymbol{\rho}_S\|^3} \\ & - (1-\mu_1)\frac{\mu_1 \boldsymbol{r} + \boldsymbol{\rho}_S}{\|\mu_1 \boldsymbol{r} + \boldsymbol{\rho}_S\|^3} + \mu_1 \frac{(1-\mu_1)\boldsymbol{r} - \boldsymbol{\rho}_S}{\|(1-\mu_1)\boldsymbol{r} - \boldsymbol{\rho}_S\|^3} \Bigg] \\ & - (1-\mu_1)\frac{\boldsymbol{\rho} + \mu_1 \boldsymbol{r}}{\|\boldsymbol{\rho} + \mu_1 \boldsymbol{r}\|^3} - \mu_1 \frac{\boldsymbol{\rho} - (1-\mu_1)\boldsymbol{r}}{\|\boldsymbol{\rho} - (1-\mu_1)\boldsymbol{r}\|^3}, \end{aligned} \tag{21}$$

where $\boldsymbol{\rho}$ and $\boldsymbol{\rho}_S$ are the nondimensional positions of the massless particle and the Sun, respectively, $\boldsymbol{r} = (1, 0, 0)^T$ is the vector from the Earth to the Moon, and C is the rotation matrix of the Earth–Moon synodic frame. Let m_E, m_M, and m_S be the masses of the Earth, Moon, and Sun, respectively, then $\mu_1 = \frac{m_M}{m_E + m_M}$ is the mass parameter of the Earth–Moon system, and $\mu_2 = \frac{m_E + m_M + m_S}{m_E + m_M}$ is a convenient way to define the mass parameter of the Sun–Earth–Moon system. Primes denote here derivatives with respect to the nondimensional time.

We obtain a set of equations that are similar to the equations of the CRTBP, and that surprisingly possesses the very same set of coefficients of the CRTBP. The BCP is hence considered as a not so small perturbation of the CRTBP, next step of the hierarchy. The major difference between the two models lays in the definition of the potential function. Indeed, the BCP potential embeds three new terms, in square brackets in Eq. (21). The first is simply due to the Sun attraction, whilst the other two stem from the nonzero acceleration of the Earth–Moon centre of mass that depends on the actual distances between the primaries and the Sun.

2.4.2. Concentric circular four-body problem

The concentric circular four-body problem, or simply CCP, is the second horizontal hierarchical part of the restricted four-body problem. It is a restricted non-coherent model that, unlike the BCP, considers one primary and two secondary bodies. It is assumed that the motion of a massless object is governed by three primaries P_1, P_2, and P_3, of masses m_1, m_2, m_3, respectively. One of the primaries is much more massive than the other two, $m_1 \gg m_2, m_3$. In a quasi-inertial reference frame centred at P_1, the bodies P_2 and P_3 rotate about m_1 in circles of radii r_2 and r_3 and with angular velocities ω_2 and ω_3, respectively. The circular orbits are coplanar. The geometry of the CCP is shown in Fig. 4

The equations of motion for P are first written as perturbation of a simple Kepler problem [31], where the main attractor is P_1.

$$\ddot{\boldsymbol{r}} + \mu_1 \frac{\boldsymbol{r}}{\|\boldsymbol{r}\|^3} = -\sum_{j=2}^{N} \mu_j \left(\frac{\boldsymbol{d}_j}{\|\boldsymbol{d}_j\|^3} + \frac{\boldsymbol{r}_{1j}}{\|\boldsymbol{r}_{1j}\|^3} \right), \tag{22}$$

where $\mu_j = Gm_j$, $\boldsymbol{d}_j = \boldsymbol{R} - \boldsymbol{R}_j$ is the distance between the massless particle and the *jth* small attractor, and $\boldsymbol{r}_j = \boldsymbol{R}_j - \boldsymbol{R}_1$ is the distance between the massive central body and the small attractors $j = 2, 3$, respectively. Eq. (22) is transformed into a P_1P_2 synodic frame by means of a proper rotation $\boldsymbol{r} = r_2 C \boldsymbol{\rho}$. The new position vector is $\boldsymbol{\rho} = (x, y, z)^T$. Dimensionless time is

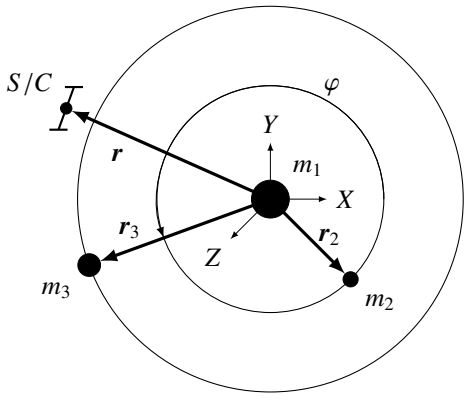

Figure 4: Geometry of the CCP in P_1-centred inertial coordinates.

again obtained through the mean motion of P_2 about P_1. The equations of motion read

$$x'' - 2y' = \Omega^{(CCP)}_{/x}, \quad y'' + 2x' = \Omega^{(CCP)}_{/y}, \quad z'' = \Omega^{(CCP)}_{/z}, \tag{23}$$

where the potential for the CCP is defined as

$$\Omega^{(CCP)} = \frac{1}{2}(x^2 + y^2) + \frac{1-\mu_1}{\|\boldsymbol{\rho}\|} + \mu_1\left(\frac{1}{\|\boldsymbol{\rho} - \boldsymbol{\rho}_2\|} + \frac{\mu_3}{\|\boldsymbol{\rho} - \boldsymbol{\rho}_3\|} + \frac{\boldsymbol{\rho}_2 \cdot \boldsymbol{\rho}}{\|\boldsymbol{\rho}_2\|^3} + \mu_3 \frac{\boldsymbol{\rho}_3 \cdot \boldsymbol{\rho}}{\|\boldsymbol{\rho}_3\|^3}\right), \tag{24}$$

and $\mu_1 = \frac{m_2}{m_1+m_2}$ is the synodic mass parameter, and $\mu_3 = \frac{m_3}{m_2}$ is the perturbation mass ratio. The position vectors of the two small attractors in the new rotating frame are

$$\boldsymbol{\rho}_2 = (1, 0, 0)^T \qquad \boldsymbol{\rho}_3, = \frac{\|\boldsymbol{r}_3\|}{\|\boldsymbol{r}_2\|}(\cos\varphi, \sin\varphi, 0)^T, \tag{25}$$

where the phase angle of P_3 with respect to the line $P_1 - P_2$ in synodic coordinates is $\varphi = \hat{\omega}t + \varphi_0$, and the apparent motion of P_3 about the synodic frame is $\hat{\omega} = \omega_3/\omega_2 - 1$. The CCP is nonautonomous due to the phase angle, φ_0.

The coefficients of the circular concentric four-body model are the very same of the CRTBP. This should not surprise because the baseline dynamics has not changed, being the well-known synodic three-body coordinates. The perturbation of the fourth body varies however the potential function.

Extreme care should be exerted when using the circular concentric problem. Indeed, due to the derivation of the motion equations, the centre of the reference frame is not the barycentre of the synodic coordinates, but it is the massive body directly, assumed to be quasi-inertial.

2.5. *Averaged coefficients*

The step before using ephemeris data to calculate the states of the celestial bodies is the creation of a database that contains the information and data on several choices of synodic reference frames. In particular the equations of motion are the same as the RPnBP, Eqs. (10). However, the coefficients are not variable functions of time, they are instead constant values that represent the average value of that coefficient for a selected pair of primaries. The average process is a time-average mathematical operator applied to the coefficients; long time spans are required to include the dynamics of all the solar system bodies. This operation avoids computing the coefficients in Eqs. (11), which is expensive. The average is applied to all the possible selection of primaries.

As an example, Tab. 1 lists the 13 coefficients of the Earth–Moon mean problem, calculated with a time average procedure on a 359.1-year span, starting from MJD 0 (i. e., 0h UT on January 1, 2000). For the sake of comparison, the table also displays the coefficients of the other gravitational models outlined so far. The mean values of the coefficients do not detach very much from the CRTBP. Perhaps, the only exception being isolated to coefficient b_{12} (see Eq. (10c)). Fig. 5 displays the absolute value maximum and minimum percent differences between some of the coefficients of the CRTBP and ERTBP, defined as

Table 1: Coefficients of the Earth–Moon restricted hierarchic models.

b_j	CRTBP BCP CCP	ERTBP	Mean model
b_1	0	0	-3.20914171488e-4
b_2	0	0	3.2232353399e-5
b_3	0	0	5.7531979499e-5
b_4	0	0	-2.992618268e-6
b_5	2	2	2.000027151596389
b_6	0	0	-1.72749153e-7
b_7	1	[0.9475, 1.0586]	1.004782125388163
b_8	0	0	5.3978293e-8
b_9	0	0	-1.25267088e-7
b_{10}	1	[0.9475, 1.0586]	1.004782657954894
b_{11}	0	0	8.5510641e-8
b_{12}	0	[−0.0586, 0.0586]	-1.612531506110e-3
b_{13}	1	[0.9475, 1.0586]	1.007472376385437

$\Delta_{\%} b_j(f, e_p) = 100 \cdot (b_j^{(CRTBP)} - b_j^{(ERTBP)})$, $j = 7, 10, 12, 13$. It can be seen that for typical primaries within the solar system (roughly 80% of primaries have $e_p < 0.1$) the eccentricity contribution does not significantly vary the coefficients of the model. However, as a critical case, the coefficients of the Sun–Mercury ERTBP exhibits variations of up to 25% with respect to those of the CRTBP.

The harmonic content of the dynamics is clearly visible in Fig. 6, displaying the Fourier transform of b_9. The peaks in the Fourier transform correspond firstly to the roto-pulsating main frequency, and secondly to the largest perturbations which affects the synodic dynamics. As for any Fourier procedure, the most relevant parameters to be specified are the size, T_0, of the sampling interval, and the number, N, of equally spaced sam-

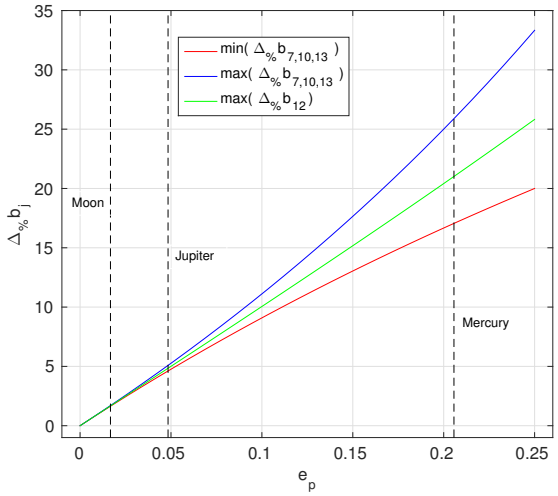

Figure 5: Extrema absolute value of the percent differences between the coefficients of the CRTBP and those of the equivalent ERTBP. Fixed eccentricity vertical lines are examples of some primaries choices within the solar system.

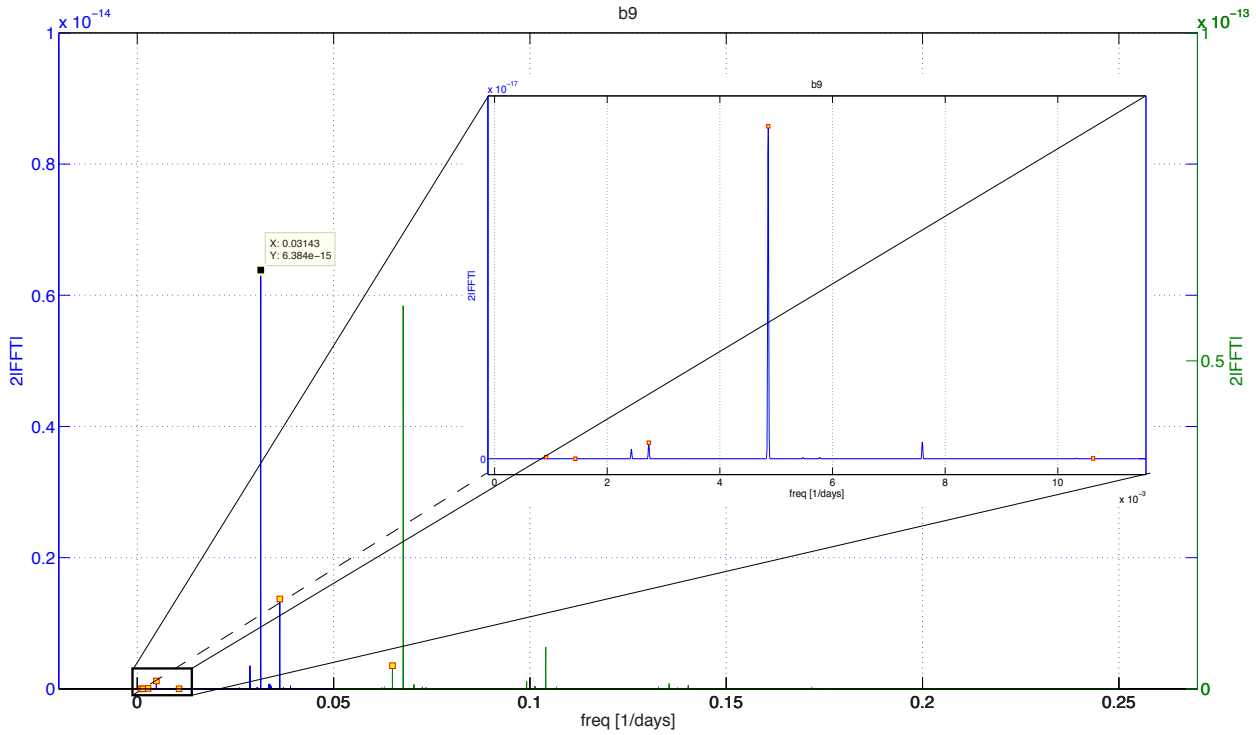

Figure 6: Norm of Fourier transform of the motion equation coefficients b_9 for the Earth–Moon case.

pling points within such interval. These parameters define the Nyquist critical frequency, $f_N = \frac{N}{2T_0}$, that fixes the window within which the frequencies (true or aliased) will be found. The number of samples has been chosen such that the Fourier analysis can detect frequencies at least equal to 1, $\frac{N}{2T_0} = 1$. Moreover, the sampling period T_0 should be large enough to allow for both being able to resolve a minimum frequency, proportional to $\frac{1}{T_0}$, and at the same time to let the solar system completely exhausts its dynamics. A period larger than 250 years suffice the purpose[2]. What is more, the number of samples chosen has been selected as a power of two in order to improve the numerical efficiency of the Fast Fourier Transform algorithm used.

As far as the Earth–Moon system is concerned, the coefficients span an interval of 359.1 years with $N = 2^{18}$ samples, which results in a time rate of 12 hours; on the other hand, the Sun– systems coefficients are sampled with $N = 2^{19}$ with a time rate of 12 hours, providing a totality of roughly 718.2 years.

Finally, in order to reduce the leakage, the functions to be transformed are truncated by means of a Hanning window function of order 2 [16],

$$H_{T_0}(t) = \frac{2}{3}\left(1 - \cos\frac{2\pi t}{T_0}\right)^2. \tag{26}$$

As expected, the majority of the perturbative contributions appear in the Fourier transform of some coefficients. Note, however, that not all the coefficients feel the same perturbative effects. For example, considering the Earth–Moon case, coefficients b_1, b_3 and b_5 show a different harmonic trend. In the Earth–Moon system, the perturbation with highest Fourier transform magnitude has period of 32 days roughly; this contribution is conjectured to be caused by the Sun.

To sum up, Fig. 7 shows the flow diagram associated to the hierarchy of the gravitational models. It's interesting to note the horizontal behaviour of the four-body models, indispensable to consider different kind of relative position for the perturbations.

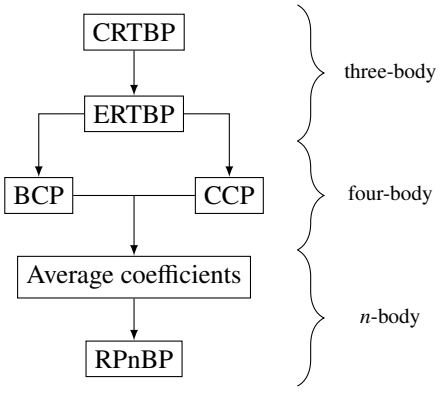

Figure 7: Hierarchic ladder for the gravitational models.

2.6. *Potential functions*

Increasing the complexity of the gravitational model in hierarchical order has lead to new dynamical equations whose coefficients do not vary significantly from the CRTBP. In the

[2]Note that Pluto has an orbital period of roughly 247 years.

BCP and CCP cases the coefficients remain even unmodified. This is because the nonlinear terms are mostly contained by a proper redefinition of the potential function, Ω. Fig. 8 shows the coloured parametric surface of section of the potential function of the BCP, on the left, and its percentage difference with the CRTBP, on the right. In order to produce a bidimensional gradient result, the height z has been set to 0. Moreover, the bicircular problem being nonautonomous, the epoch has been chosen at the date March 11 2015, $12^{hr}56^{m}00^{s}$ TDB. With this choice the initial phase angle of the Sun with respect to the Earth–Moon line is roughly 115°. Several tests have been run with different epochs within a lunar period. The areas of minimum and maximum percentage variation follow the Sun direction (black arrow in Fig. 8) and the whole picture rotates counterclockwise. Except this rotating variation, the main shape of the potential seems not to vary significantly within roughly 28 days from the result presented on the right figure.

The typical regions of motion associated to the Jacobi constant are maintained. The surfaces of zero-velocity, even though now are variable, have retained the typical progression shape: oval, dumbbell, horseshoe, and tadpole. The fundamental difference is that the perturbation of the Sun creates regions at higher and lower levels of potential. The main consequence is that there exist special configurations of the spacecraft at certain epoch where the energy required to escape the Earth–Moon attraction and open the passage at L_1 and L_2 is lower. Conversely, the opposite behaviour exists as well; the Sun can indeed act upon the spacecraft to favour the stability of a capture orbit in the synodic system. It is very peculiar to see how the action of the Sun is symmetric. The central region has very low values of variation, and bifurcates along the direction normal to the Sun resulting in bigger regions with negative variation of potential. The remaining regions, clustered in the Sun and anti-Sun directions have positive variation of potential. The small boundary regions of the saddle that have zero variation of potential are the regions where the perturbation of the Sun does not play any role in the vector field of the massless particle, and presumably are the best conditions to propagate halo-type orbits.

3. METHODOLOGY

In this Section the attention is focused on the logical and mathematical procedure to continue trajectories calculated in the CRTBP toward the RPnBP. The selection of the orbit to refine is based on two factors: the stability of the orbit within the three-body frame, and the sensibility to the increased chaotic content associated to the larger number of retained celestial bodies.

Interplanetary transfers and halo-like orbits are deemed to satisfy these requirements, and, on top of that, they are being widely used for current space missions. The computation of halos must account for the non-linear terms that arise in the linearised CRTBP when large amplitude orbits are considered. These solutions are obtained through a numerical approach, based on *perturbation techniques* [24], in order to correct the analytic initial estimates, and on *continuation techniques* [18], in order to expand the infinitesimal orbits. halo orbits are periodic orbits which bifurcate from the planar Lyapunov orbits when the in-plane and out-of-plane frequencies of the linearised vector field are equal. This is a 1:1 resonance that appears as a consequence of the nonlinear terms of the equations and, hence, these 1-D invariant tori have to be searched as series expansion with a single frequency. In details, once the out-of-plane A_z amplitude overcomes a limit value, the frequency of the in-plane oscillatory motion achieves the value of the frequency of the one out of the plane, and three-dimensional halo orbits emerge. Fig. 9 represents a family of halo orbits of the L_1 Sun-Jupiter system, calculated via high-order differential corrections [30].

In this work, a *Lindstedt-Poincare method* is used to accurately compute periodic and quasi-periodic trajectories around a libration point. This process is based on finding a parametric family of trigonometric expansions that satisfy the equations of motion, up to a sufficiently high order. The potential function is expanded by means of Taylor series and terms up to the second order have been retained. According to [24], Legendre polynomial are used to retain high-order terms. The solution of the linear periodic part of these equations remains unvar-

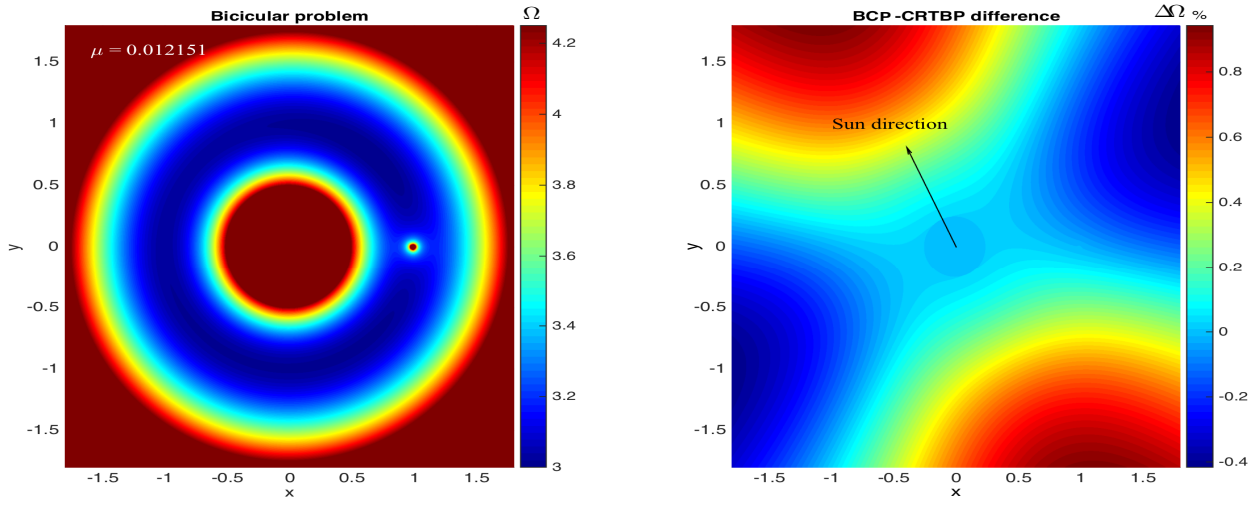

Figure 8: Potential function, $\Omega(x, y, 0)$, colour-gradient visualisation.

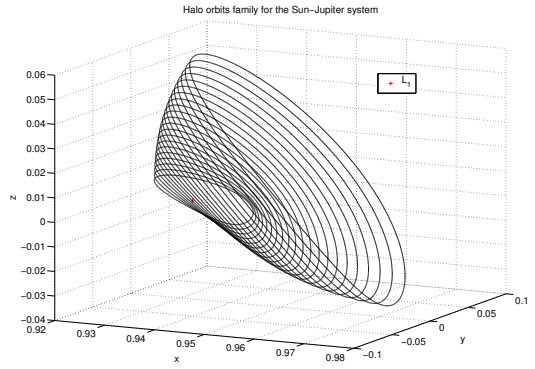

Figure 9: Halo orbits family around the first collinear point L_1 of the Sun–Jupiter system.

ied. These linear solutions are already Lissajous trajectories. Following the procedure in [12], when the nonlinear terms (in Legendre polynomials form) are considered, the complete solution is sought as formal series in powers of the amplitudes A_x and A_z.

The main objective is to continue these halo orbits in the RPnBP exploiting the hierarchy of the gravitational models to smooth the nonlinear terms gradients and to ensure the success of the refinement procedure. These orbits have been already demonstrated to exist in the complete ephemeris model [17], even though with small quasi-periodic modification in the baseline shape and oscillation frequency. However, the computation of these trajectories is computationally very expensive and requires an ad-hoc procedure that is very cumbersome from the mathematical perspective and that can fail according to the precision of the initial condition and to the time scale used. We argue that this is because the passage from CRTBP to RPnBP is too sharp, and the algorithm might encounter difficulties in the minimisation of the objective function at hand. Applying the same algorithm sequentially from the CRTBP to the RPnBP and following the hierarchic order of the gravitational models established in this paper, convergence is attained and the algorithm is prone to easily find local optima that satisfy the requirements.

The refinement procedure, inspired by [22, 8], is achieved by means of an iterative algorithm that consists of two steps: *evaluation of a compliant initial seed orbit*, and *modified multiple shooting*.

The two-point boundary value problem (TPBVP) is formulated slightly different from usual, leading to the name modified multiple shooting. In particular, the technique has to cope with the fact that no boundary conditions are actually known, and the sole requirement is to produce a piecewise continuous trajectory which stays as 'close' as possible in phase space to the initial seed. In order to attain this, the multiple shooting is coupled with an optimisation. In the first place, the classical optimal problem is translated into a *non-linear programming* (often termed NLP) method by means of direct transcription of the dynamics and the problem is then solved for a finite set of variables when a proper objective function is specified [3, 6]. As opposite to the optimal control problem, no dynamics is involved into a NLP problem, because in this case the dynamics is merely seen as a constraint that the NLP must satisfy. Let T_0 be the initial epoch, which should be specified due to the nonautonomous nature of the n-body problem, and ΔT the time-span covered by a certain set of nodes. The basic procedure for trajectory refinement consists basically of the following steps:

Step 1 Using a simplified gravitational model, generate a sequence of nodes as initial guess for *Step 2*;

Step 2 Fix the initial epoch, T_0, and for a given time-span ΔT, perform the modified multiple shooting with the initial guess.

3.1. The modified multiple shooting

A TPBVP consists in finding $\mathbf{x}(t)$, $t \in [t_0, t_f]$, such that

$$\dot{\mathbf{x}} = \mathbf{f}(\mathbf{x}, t), \qquad \mathbf{h}(\mathbf{x}(t_0), \mathbf{x}(t_f)) = \mathbf{0}. \tag{27}$$

In the present context, the first equation is the state space representation of Eqs. (10) ($\boldsymbol{x}$ is 6-dimensional) when the proper coefficients b_j and potential function Ω are specified according to the selected dynamical model as described in Section 2. The function $\mathbf{h}$ specifies six boundary conditions, which are needed to well-pose the problem [4]. In multiple shooting, problem (27) is solved for a finite set of variables [23]. The procedure is briefly recalled here for convenience.

The solution is discretised over m points $t_0 = t_1 < t_2 < \cdots < t_m = t_f$; that is, $\mathbf{s}_k = \mathbf{x}(t_k)$, $k = 1, \ldots, m$. This defines $m - 1$ segments in which a TPBVP is solved by enforcing continuity of the solutions at both ends. This shortens the duration of the original problem, and thus reduces sensitivity. Let the defect vector be

$$\boldsymbol{\zeta}_k = \boldsymbol{\varphi}(\mathbf{s}_k, t_k; t_{k+1}) - \mathbf{s}_{k+1}, \quad k = 1, \ldots, m-1, \tag{28}$$

where $\boldsymbol{\varphi}(\boldsymbol{x}_0, t_0; t)$ is the flow (i. e., solution) at time t of Eq. (27) starting from initial conditions $(\boldsymbol{x}_0, t_0)$. A schematic representation of the defect vectors is shown in Fig. 10. The problem is to determine the states $\mathbf{s}_k$ such that

$$\boldsymbol{\zeta}_k = \mathbf{0}, \quad k = 1, \ldots, m-1, \quad \text{and} \quad \mathbf{h}(\mathbf{s}_1, \mathbf{s}_m) = \mathbf{0}. \tag{29}$$

In Eqs. (29) we have $6m$ unknowns (the states $\mathbf{s}_k$) and $6m$ equations (6 boundary conditions and $6(m-1)$ defect constraints). This is the classic multiple shooting method.

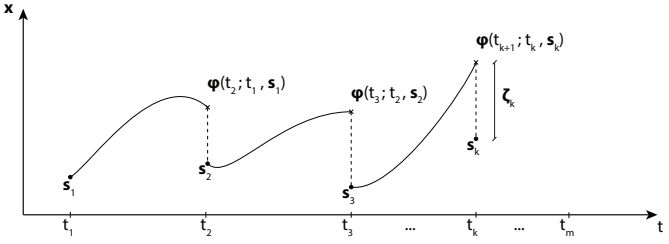

Figure 10: Multiple shooting strategy and defects vector.

In the modified version of the multiple shooting the fundamental principles of the classical technique are preserved, and eventually the zero of a non-linear multi-variable function has to be found by Newton method. However, the classic multiple shooting has be be modified so as to deal with free boundary conditions. In particular, the equations that represent the boundary conditions, $\boldsymbol{h}$, are erased. Let $\mathbf{s} = (\mathbf{s}_1, \mathbf{s}_2, \ldots, \mathbf{s}_m)$ be the vector of unknowns and let

$$\mathbf{c}(\mathbf{s}) = \begin{bmatrix} \boldsymbol{\zeta}_1(\mathbf{s}_1, \mathbf{s}_2) \\ \boldsymbol{\zeta}_2(\mathbf{s}_2, \mathbf{s}_3) \\ \vdots \\ \boldsymbol{\zeta}_{m-1}(\mathbf{s}_{m-1}, \mathbf{s}_m) \end{bmatrix} \tag{30}$$

be the vector of defects.

Note that $\mathbf{c}(\mathbf{s}) : \mathbb{R}^{6m} \to \mathbb{R}^{6(m-1)}$ and $\mathbf{s} \in \mathbb{R}^{6m}$. We have to seek the zero of the function $\mathbf{c}(\mathbf{s})$, while minimising a scalar objective function $f(\mathbf{s}) : \mathbb{R}^{6m} \to \mathbb{R}^1$, defined later. An optimisation procedure is implemented in order to shatter the underdetermination and provide for the 6 missing equations. The problem is stated as

$$\min_{\mathbf{s}} f(\mathbf{s}) \quad \text{subject to} \quad \mathbf{c}(\mathbf{s}) = \mathbf{0}. \tag{31}$$

In order to minimise the deviation between the final trajectory and the seeding one, the cost function f is chosen to be a quadratic form of the constraints,

$$f(\mathbf{s}) = \frac{1}{2}\mathbf{c}^T\mathbf{c}. \tag{32}$$

Note that this also lead to minimising the corrections applied by the modified multiple shooting.

The problem is solved numerically. The Jacobian of the function $\mathbf{c}$, $\mathcal{J}_c$, is calculated by means of a first-order Euler approximated forward finite difference scheme. This method has been preferred over more accurate techniques (i. e., second-order centred finite difference schemes or variational equations) for implementation simplicity and reliability. The Jacobian is sparse:

$$\mathcal{J}_c(\mathbf{s}) = \begin{bmatrix} \Phi_1 & -\mathcal{I}_6 & 0 & & 0 \\ 0 & \Phi_2 & -\mathcal{I}_6 & \ddots & \\ & \ddots & \ddots & \ddots & 0 \\ 0 & & \ddots & \Phi_{m-1} & -\mathcal{I}_6 \end{bmatrix}, \tag{33}$$

where $\mathcal{I}_6$ is the identity matrix of order 6, the state transition matrices Φ_k are given by

$$\Phi_k = \mathcal{D}_{\mathbf{s}_k}\boldsymbol{\zeta}_k = \mathcal{D}_{\mathbf{s}_k}\boldsymbol{\varphi}(t_{k+1}; t_k, \mathbf{s}_k), \tag{34}$$

and $\mathcal{D}_{\mathbf{s}_k}(\cdot)$ is the gradient with respect to $\mathbf{s}_k$.

Basically, the method consists of three steps:

1. Select and calculate trajectory to be refined;
2. Apply the continuation method to make a step further in the hierarchic ladder and update the initial conditions;
3. Reiterate until the top of the hierarchic ladder, i. e., RPnBP.

4. RESULTS

The method described in Section 3 is applied to three families of trajectories: (a) a family of halo orbits in the Earth–Moon system at three different Jacobi constants; (b) an Earth-to-Moon Hohmann transfer; and (c) an Earth-to-Moon low-energy transfer that exploits the weak stability boundaries of the lunar region. The initial conditions for both Earth-to-Moon transfers have been taken from [29].

4.1. Refinement of halo orbits

The initial condition for a Earth–Moon L_1 halo orbit are flown under the vector gravitational fields in the hierarchy. As expected, the CRTBP reproduces again the original halo orbit. Within the other dynamics, the orbit deviates from the original path and follows different trajectories, which might in some cases be substantially different from the expected quasi-periodic behaviour. This is because the other celestial bodies produce perturbation along the orbit that are not negligible. Fig. 11 shows the propagation of the halo orbits in the different dynamical models. The BCP stays very close to the CRTBP, making more than a complete revolution along the halo orbit before escaping towards the Earth. This happens because at the selected initial time the perturbation of the Sun is minimum along the trajectory. However, as time passes the Earth–Moon system revolves about the Sun, whose action eventually pulls away the orbit. The RPnBP and the ERTBP behave in similar fashion near the libration point, but detaches very quickly from the halo trajectory and are temporarily captured in a selenocentric orbit. These two models produce similar results because at such distances the effect of the eccentricity of the lunar orbit produces greater effects than the solar gravity. Lastly, the averaged coefficients model is not able to simulate the nonlinearity of the gravitational field, and results in a very fast escape from the desired configuration. This model should be used with extreme care. In fact, when following the chain of models it has produced convergence issues for the refinement of the larger halo orbits. In the latter cases, the average coefficient models is not representative of the real dynamics. Conversely, for smaller LPOs the vector field is closer to the real scenario. This is conjectured to occur mainly because the value of b_{13} equally scales the potential gradient (which in this model comprehend the contributions of the other n bodies) in every point of the phase space.

The continuation algorithm is applied to Earth–Moon L_1 halo orbits, associated to different amplitude parameters, A_z of the northern family (first coefficient of the Fourier expansion of the z-coordinate in normalised units, in which the unit length is taken as the distance between the libration point and the secondary). Different values of A_z univocally correspond to different energy levels, and thus to different values of the Jacobi constant. Given any of these two parameters, one particular halo orbit is specified. Results are presented in Fig. 12, which displays the refinement of three halo orbits about the Earth–Moon first libration point, associated to three different values of the amplitude, $A_z = (0.01, 0.03, 0.06)$. Note that larger amplitude means larger orbital path, and therefore smaller Jacobi energy,

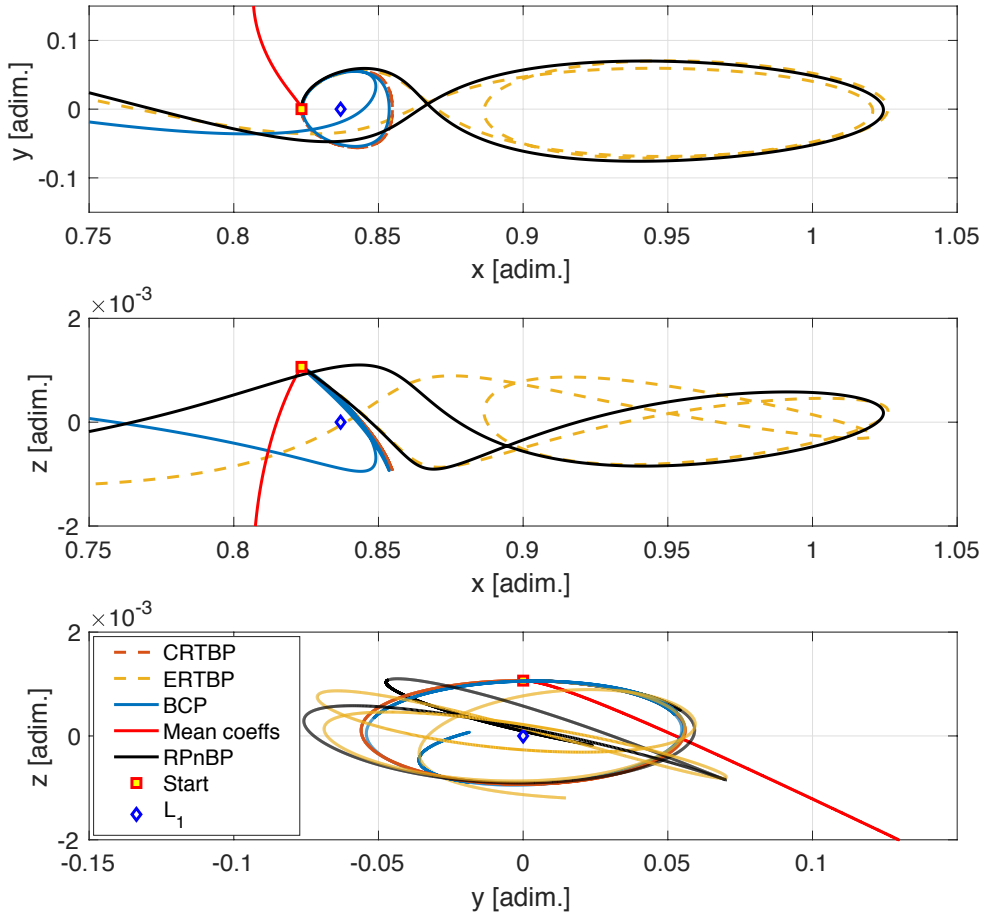

Figure 11: $x-y$ (top), $x-z$ (middle), $y-z$ (bottom) projections of a Earth–Moon $A_z = 384.4$ km halo, propagated in different gravitational models.

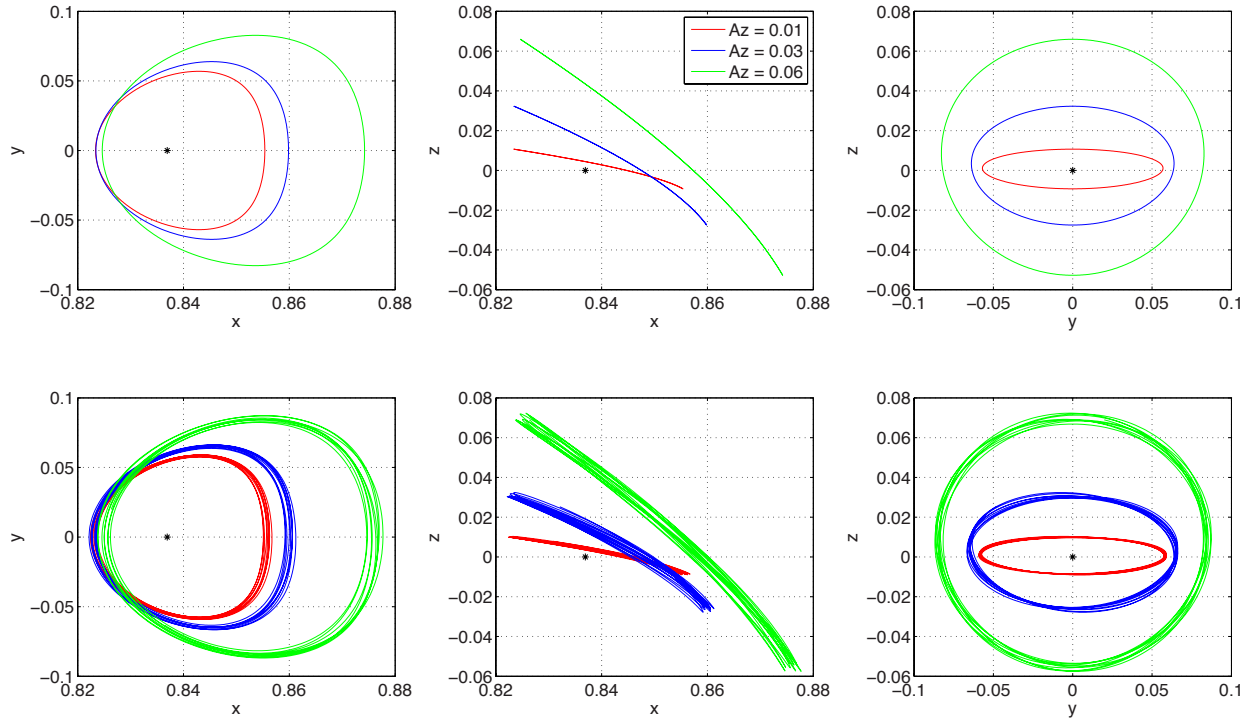

Figure 12: Initial CRTBP guess (top) and refinement (bottom) of halo orbits with $A_z = 0.01$ (smallest orbit), $A_z = 0.03$, and $A_z = 0.06$ (largest orbit) of the Earth-Moon L_1 libration point. Only the first year is plotted.

C_J. The refinement has been done for 150 primaries revolutions, but for the sake of presentation clarity, only the first year is graphed. It is clear that the numerical refinement procedure of a halo orbit produces a quasi-periodic one, whereas the baseline shape and size do not change for most of the cases.

The advantage of this algorithm is its simplicity. Using a hierarchic modelling chain of increasing complexity in order to go from a CRTBP-like model to the RPnBP prevents the application of interpolation/extrapolations steps that might be necessary to attain convergence if a direct continuation from the CRTBP to the RPnBP is performed (see [22]). This is because the transition among models is smoother, the optimisation is well-behaved, and convergence properties more ideal. This effect increases for larger time spans. Nevertheless, both Andreu [1] and Lian et al. [22] obtain orbits of different kinds (e. g., larger time spans, planar and vertical Lyapunov, halo and quasi-halo, and around different libration points) directly from the CRTBP within the restricted n-body problem, without passing through the hierarchy of models. The algorithm introduced in this work approach the same refinement problem with a different methodology, and is applied also to end-to-end interplanetary trajectories.

The results obtained here, that is quasi-periodic orbits around the Earth–Moon L_1, have also been compared with the ones obtained in [22] with a different method. This benchmark has shown how the refined trajectories of these two works are very close.

A Fourier analysis of the refined halo-type orbit shows that the main single halo frequency is maintained. In addition, since the refined orbit is now quasi-periodic, other frequencies appear. In particular, the frequency corresponding to main gravitational perturbers appear. Note that the perturbative effects of other massive planets are present, but cannot be resolved by the Fourier transform due to the limited total period.

Fig. 13 shows the evolution of the smaller halo orbit refinement in the ERTBP, BCP, and RPnBP. Only some of the multiple shooting legs are displayed for clarity of presentation. It is very interesting to note that, depending on the actual position of the Sun with respect to the Earth–Moon system, the BCP does not always better represent the vector field if compared to the ERTBP. In particular, in the left part of the displayed trajectory the ERTBP is closer to the actual quasi-periodic refined orbit in the RPnBP. This occurs even though, on average, climbing up the hierarchic ladder of dynamical model produces results that are more and more accurate and closer to the real n-body problem.

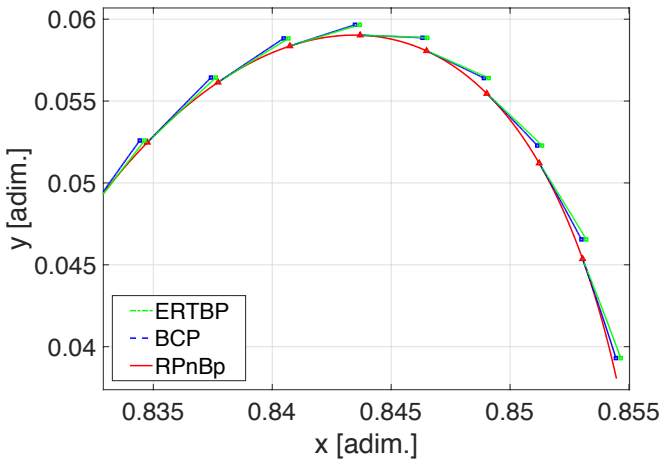

Figure 13: Multiple shooting legs for the refinement of the $A_z = 0.01$ halo orbit in three different models within the hierarchic ladder (ERTBP, BCP, and RPnBP).

4.2. *Refinement of Earth-to-Moon transfers*

Two sets of initial conditions for optimal two-impulse Earth–Moon transfers [29] are flown under the gravitational fields in the hierarchy. The trajectories are labeled as Hohmann transfer and weak stability boundary transfer, respectively. While the Hohmann transfer is computed in the CRTBP and can thus be refined following the nominal hierarchical ladder of dynamical models, the WSB transfer has been designed in a four-body model and the refinement is performed exploiting only the BCP and the RPnBP. In both cases, the S/C arrives at the Moon on a circular orbit at 100 km altitude, and departs the Earth on a ellipse with $653 \times 70,000$ km periapsis/apoapsis altitude. The Hohmann transfer employs 3.47 days to reach the Moon, while 75.57 days are necessary for the low-energy transfer.

The first row of Fig. 14 displays the evolution of the transfers refinement for different dynamical models in the hierarchy. The trajectories are plotted in the Earth–Moon synodic frame. The Hohmann transfer is sampled in four multiple shooting segments, for which Fig. 14a shows the behaviour within the ERTBP, BCP, and average coefficient model. Clearly, the earth departure leg is not well-captured by the elliptic problem, which however produces results that are compatible with the initial orbit in the coasting phase and Moon arrival leg. The BCP is remarkably close to the optimal solution. The results of the average coefficients model are not satisfactorily and are not used effectively during the refinement process. This suggests that a simple average on the 13 coefficients is not sufficient to represent correctly the dynamical behaviour of the real ephemeris n-body problem. For the WSB transfer, divided in 13 equally spaced multiple shooting segments of roughly 5.8 days each, the BCP sticks very close to the optimal trajectory, while the elliptic model deviates from the nominal path for longer distances.

The first guess and final refined solutions for the Hohmann and WSB transfers are shown in Fig. 14c and Fig. 14d, respectively. The states of departure and arrival are hard boundary conditions the multiple shooting target, while tweaking the epochs of departure and arrival. In both cases, the transfers have been successfully refined in the real ephemeris roto-pulsating n-body problem.

5. CONCLUSION

In this paper an algorithm has been developed, that continues and refines trajectories calculated in the CRTBP (or slightly more involved dynamical models) towards the more comprehensive ephemeris-based roto-pulsating n-body problem. The

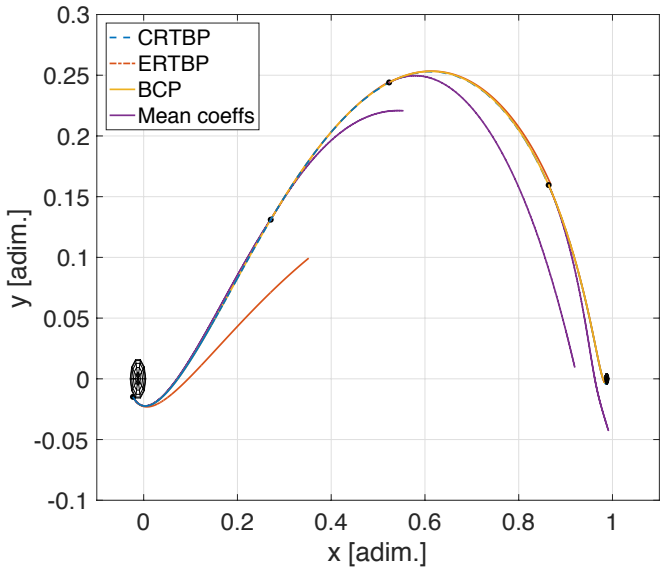

(a) Hohmann transfer evolution in different dynamical models.

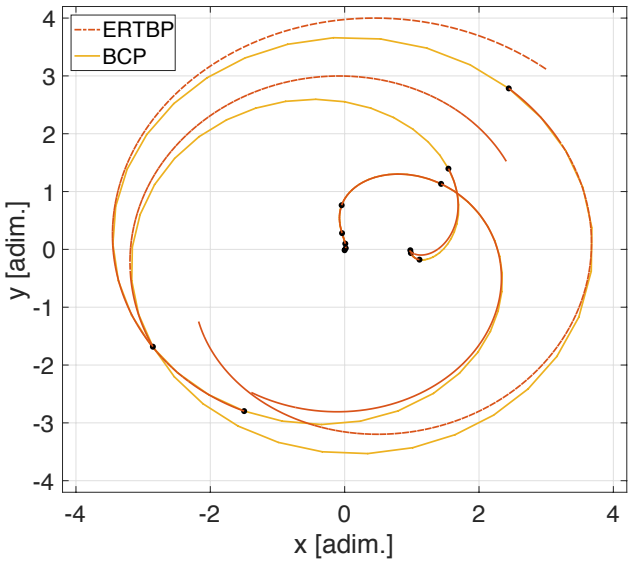

(b) Low-energy WSB transfer evolution in the ERTBP and BCP.

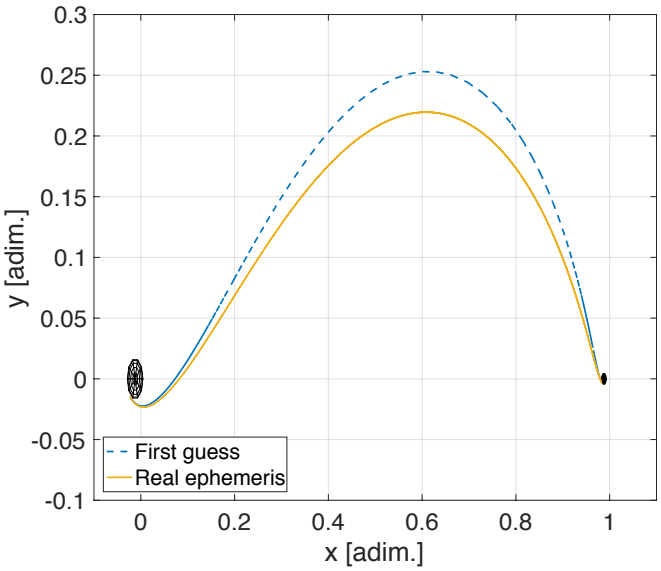

(c) First guess and refined solutions for the Earth–Moon Hohmann trajectory.

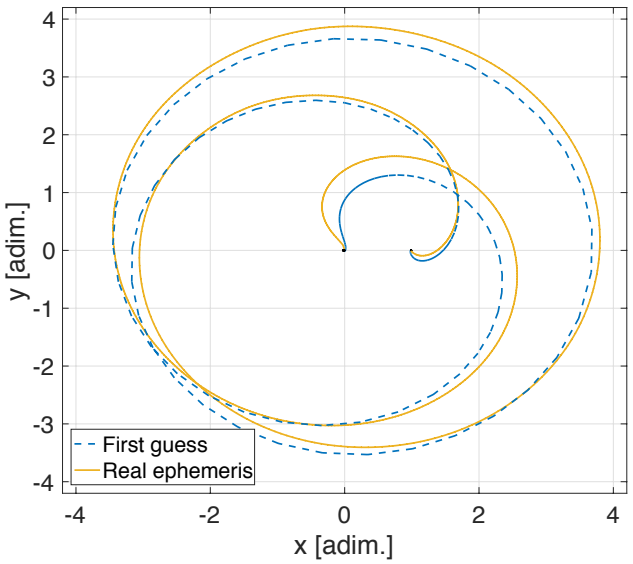

(d) First guess and refined solutions for the Earth–Moon WSB trajectory.

Figure 14: Refinement of Hohmann (first column) and low-energy WSB (second column) Earth–Moon transfers.

intrinsic hierarchic behaviour of the gravitational models at hand has been employed to attain convergence and to improve the efficiency of the algorithm. The difference among various vector fields has been made smoother with a progressive increase of the dynamical models complexity, explicitly using a hierarchic approach. In particular, a family of three Earth–Moon L_1 halo orbits have been refined with the proposed method. The refinement algorithm has also been successfully applied to two optimal Earth–Moon transfers, a direct Hohmann-like transfer and a low-energy transfer using weak stability boundary of the Sun–Earth–Moon system. The test cases show the validity of the algorithm when compared to similar methods in which the gravitational models hierarchy is not explicitly exploited.

Acknowledgements

The first author would like to thank the Italian Space Agency, ASI, and the Space Generation Advisory Council, SGAC, for the grant to attend the IAC 2015 and the Space Generation Congress 2015, where this work has been first presented.

Bibliography

[1] Andreu, M. A., 1998. The quasi-bicircular problem. Ph.D. thesis, Univ. Barcelona.

[2] Belbruno, E., Miller, J., 1990. A ballistic lunar capture trajectory for the japanese spacecraft Hiten. Jet Propulsion Laboratory, IOM 312, 90–4.
[3] Betts, J. T., 2010. Practical methods for optimal control and estimation using nonlinear programming, 2nd Edition. Philadelphia, PA : Society for Industrial and Applied Mathematics.
[4] Bolle, A., Circi, C., 2012. A hybrid, self-adjusting search algorithm for optimal space trajectory design. Advances in Space Research 50 (4), 471–488.
[5] Conley, C. C., 1968. Low energy transit orbits in the restricted three-body problems. SIAM Journal on Applied Mathematics 16 (4), 732–746.
[6] Conway, B. A., 2010. Spacecraft trajectory optimization. Vol. 32. Cambridge University Press Cambridge, UK.
[7] Dei Tos, D. A., 2014. Automated trajectory refinement of three-body orbits in the real solar system model. Master's thesis, Politecnico di Milano.
[8] Dei Tos, D. A., Topputo, F., 2015. On the advantages of using a strict hierarchy to model astrodynamical problems. In: 66th International Astronautical Congress, Jerusalem, Israel. pp. 1–12.
[9] Dei Tos, D. A., Topputo, F., 2017. Trajectory refinement of three-body orbits in the real solar system model. Advances in Space Research.
[10] Folkner, W. M., Williams, J. G., Boggs, D. H., Park, R. S., Kuchynka, P., 2014. The planetary and lunar ephemerides DE430 and DE431. Tech. rep., JPL Interplanetary Network Progress Report 42-196.
[11] García, F., Gómez, G., 2007. A note on weak stability boundaries. Celestial Mechanics and Dynamical Astronomy 97 (2), 87–100.
[12] Gómez, G., Masdemont, J. J., Mondelo, J. M., 2002. Libration point orbits: a survey from the dynamical point of view. World Scientific, Ch. 16, pp. 311–372.
[13] Gómez, G., Masdemont, J. J., Mondelo, J. M., 2002. Solar system models with a selected set of frequencies. Astronomy and Astrophysics 390 (2), 733–750.
[14] Gómez, G., Masdemont, J. J., Mondelo, J. M., 2003. Dynamical substitutes of the libration points for simplified Solar system models. World Scientific, Ch. 17, pp. 373–397.
[15] Gómez, G., Mondelo, J. M., 2001. The dynamics around the collinear equilibrium points of the rtbp. Physica D: Nonlinear Phenomena 157 (4), 283–321.
[16] Harris, F. J., Jan 1978. On the use of windows for harmonic analysis with the discrete fourier transform. Proceedings of the IEEE 66 (1), 51–83.
[17] Hou, X. Y., Liu, L., 2011. On quasi-periodic motions around the collinear libration points in the real earth–moon system. Celestial Mechanics and Dynamical Astronomy 110 (1), 71–98.
[18] Howell, K. C., Pernicka, H. J., 1987. Numerical determination of lissajous trajectories in the restricted three-body problem. Celestial mechanics 41 (1), 107–124.
[19] Hyeraci, N., Topputo, F., 2010. Method to design ballistic capture in the elliptic restricted three-body problem. Journal of guidance, control, and dynamics 33 (6), 1814–1823.
[20] Jehn, R., Campagnola, S., Garcia, D., Kemble, S., 2004. Low-thrust approach and gravitational capture at mercury. In: 18th International Symposium on Space Flight Dynamics. Vol. 548. p. 487.
[21] Jorba, A., Masdemont, J. J., 1999. Dynamics in the center manifold of the collinear points of the restricted three body problem. Physica D: Nonlinear Phenomena 132 (1), 189–213.
[22] Lian, Y. J., Gómez, G., Masdemont, J. J., Tang, G. J., 2013. A note on the dynamics around the lagrange collinear points of the earth–moon system in a complete solar system model. Celestial Mechanics and Dynamical Astronomy 115 (2), 185–211.
[23] Mingotti, G., Topputo, F., Bernelli-Zazzera, F., 2012. Transfers to distant periodic orbits around the Moon via their invariant manifolds. Acta Astronautica 79, 20–32.
[24] Richardson, D. L., 1980. Analytic construction of periodic orbits about the collinear points. Celestial mechanics 22 (3), 241–253.
[25] Russell, R. P., Lam, T., 2007. Designing ephemeris capture trajectories at europa using unstable periodic orbits. Journal of guidance, control, and dynamics 30 (2), 482–491.
[26] Sousa Silva, P. A., Terra, M. O., 2012. Applicability and dynamical characterization of the associated sets of the algorithmic weak stability boundary in the lunar sphere of influence. Celestial Mechanics and Dynamical Astronomy 113 (2), 141–168.
[27] Szebehely, V., 1967. Theory of orbits: the restricted problem of three bodies. Academic Press, New York.
[28] Tang, G., Gomez, G., Masdemont, J. J., Yijun, L., et al., 2013. A note on the dynamics around the l1, 2 lagrange points of the earth-moon system in a complete solar system model. Celestial Mechanics and Dynamical Astronomy 15 (2), 185–211.
[29] Topputo, F., 2013. On optimal two-impulse earth–moon transfers in a four-body model. Celestial Mechanics and Dynamical Astronomy 117 (3), 279–313.
[30] Topputo, F., 2016. Fast numerical approximation of invariant manifolds in the circular restricted three-body problem. Communications in Nonlinear Science and Numerical Simulation 32, 89 – 98.
[31] Vallado, D. A., 2001. Fundamentals of astrodynamics and applications. Vol. 12. Springer.